# Ionic Transport and Charge Distribution in Miniaturized Electrochemical Energy Storage Devices by Modeling Investigation

Yannick Dufil, Frederic Favier, Thierry Brousse, Christophe Lethien, Jean Le Bideau, Olivier Fontaine

▶ **To cite this version:**

Yannick Dufil, Frederic Favier, Thierry Brousse, Christophe Lethien, Jean Le Bideau, et al.. Ionic Transport and Charge Distribution in Miniaturized Electrochemical Energy Storage Devices by Modeling Investigation. Journal of The Electrochemical Society, 2022, 169 (6), pp.060551. 10.1149/1945-7111/ac7a65 . hal-03706957

**HAL Id: hal-03706957**
**https://hal.science/hal-03706957**

Submitted on 13 Jul 2022

**HAL** is a multi-disciplinary open access archive for the deposit and dissemination of scientific research documents, whether they are published or not. The documents may come from teaching and research institutions in France or abroad, or from public or private research centers.

L'archive ouverte pluridisciplinaire **HAL**, est destinée au dépôt et à la diffusion de documents scientifiques de niveau recherche, publiés ou non, émanant des établissements d'enseignement et de recherche français ou étrangers, des laboratoires publics ou privés.

Journal of The Electrochemical Society

The Electrochemical Society
Advancing solid state & electrochemical science & technology

**ACCEPTED MANUSCRIPT**

# Ionic Transport and Charge Distribution in Miniaturized Electrochemical Energy Storage Devices byModeling Investigation

To cite this article before publication: Yannick Dufil *et al* 2022 *J. Electrochem. Soc.* in press https://doi.org/10.1149/1945-7111/ac7a65

Manuscript version: Accepted Manuscript

Accepted Manuscript is "the version of the article accepted for publication including all changes made as a result of the peer review process, and which may also include the addition to the article by IOP Publishing of a header, an article ID, a cover sheet and/or an 'Accepted Manuscript' watermark, but excluding any other editing, typesetting or other changes made by IOP Publishing and/or its licensors"

This Accepted Manuscript is **© 2022 The Author(s). Published by IOP Publishing Ltd.**.

This article can be copied and redistributed on non commercial subject and institutional repositories.

Although reasonable endeavours have been taken to obtain all necessary permissions from third parties to include their copyrighted content within this article, their full citation and copyright line may not be present in this Accepted Manuscript version. Before using any content from this article, please refer to the Version of Record on IOPscience once published for full citation and copyright details, as permissions will likely be required. All third party content is fully copyright protected, unless specifically stated otherwise in the figure caption in the Version of Record.

View the article online for updates and enhancements.

This content was downloaded from IP address 193.54.110.51 on 27/06/2022 at 07:32

# Ionic Transport and Charge Distribution in Miniaturized Electrochemical Energy Storage Devices by Modeling Investigation

| | |
|---|---|
| Journal: | *Journal of The Electrochemical Society* |
| Manuscript ID | JES-107343.R1 |
| Manuscript Type: | Research Paper |
| Date Submitted by the Author: | 08-Jun-2022 |
| Complete List of Authors: | Dufil, Yannick; ICGM<br>Favier, Frederic; University of Montpellier Faculty of Sciences, Institut Charles Gerhardt Montpellier UMR 5253 CNRS-UM-ENSCM<br>Brousse, Thierry; Institut des Mat&#65533;riaux Jean Rouxel (IMN) University of Nantes/CNRS, Polytech Nantes<br>Lethien, christophe; IEMN,<br>Le Bideau, Jean; Institut des Materiaux Jean Rouxel<br>Fontaine, Olivier; VISTEC, chemistry |
| Keywords: | charge heterogeneity, Null material, microbattery, COMSOL |
| | |

SCHOLARONE™
Manuscripts

Accepted Manuscript

# Ionic Transport and Charge Distribution in Miniaturized Electrochemical Energy Storage Devices by Modeling Investigation

Yannick Dufil,[1] Frederic Favier,[1,6] Thierry Brousse,[2,6,*] Christophe Lethien,[3,6] Jean Le Bideau,[2,6] Olivier Fontaine[4,5,z]

[1]ICGM, Univ Montpellier, CNRS, ENSCM, Montpellier, France.

[2]Université de Nantes, CNRS, Institut des Matériaux Jean Rouxel, IMN, 44000 Nantes, France

[3]Univ. Lille, CNRS, Univ. Polytechnique Hauts-de-France, UMR 8520 - IEMN - Institut d'Electronique de Microélectronique et de Nanotechnologie, F-59000 Lille, France

[4]School of Energy Science and Engineering, Vidyasirimedhi Institute of Science and Technology (VISTEC), Rayong 21210, Thailand.

[5]Institut Universitaire de France, 75005 Paris, France.

[6]Réseau sur le Stockage Electrochimique de l'Energie, CNRS FR 3459, 80039 Amiens Cedex, France

[*]Electrochemical Society Member.

[z]E-mail: olivier.fontaine@vistec.ac.th

Accepted Manuscript
For Review Only

**Abstract**

Ions are at the core of the mechanism involved in electrochemical energy storage. However, it remains difficult to physically measure the local ionic transport inside working devices. Limiting factors in the local transport in Miniaturized Electrochemical Energy Storage (MEES), especially in 3D Li-ion microbatteries, are investigated using finite element modeling with COMSOL Multiphysics®. This work aims to lay the basements for establishing a relationship between the main limiting factors of Li-ion microbatteries, to provide the critical points for designing the efficient microstructures. Contrary to what was reported in the literature, we demonstrate that the electronic conductivity of the electrodes does not play such a significant role in limiting the performance of a Li-ion microbattery. We show that the main limiting factor is the ionic diffusion inside the electrode, and also the geometry and charge applied to the battery (Crate) which are closely related to ionic diffusion in the electrode.

Accepted Manuscript
For Review Only

## Introduction

The development of miniaturized electrochemical energy storage systems is crucial for the growth of onboard electronic devices and sensors, that will help improve the intelligent and connected devices increasingly deployed worldwide.[1,2] There is a gap between the growing demand for inexpensive, reliable, and efficient miniaturized energy storage systems (MEES) and what the market offers.[3–6] Within large-scale electrochemical energy storage systems and MEES, there are numerous ionic exchanges at the electrode/electrolyte interface.

Flat Li-ion or lithium-based microbatteries currently lack power and energy density.[2,7] To overcome these issues, research has focused on reducing the electrode thickness (to increase the power density) and increasing the surface developed by the electrodes and the electrolyte, with a method of building 3D microstructures (to enhance the energy density).[8–10] These MEES are generally named 3D microbatteries (3D-Mbs). 3D-Mbs are currently under investigation with 3D scaffolds ranging, from trench[11] to nanostructured interdigitated systems[12], which will be discussed here in the first part of this paper. However, there is a lack of formalism in describing the relationship between the various properties of the materials with the geometry used. This is the driving force that leads us to develop a modeling approach to identify the main factors limiting the 3D-Mbs performance. A mathematical model of a so-called trench cell has been developed. The model has been strengthened and complexified to better account for the physical-chemical phenomena taking place in the cell. This advanced model should point out the key parameters to be considered together, and that for designing more efficient microstructures.

We began our study with precise classification of the various available geometries, revealing two reference architectures: planar and stacked. We used finite element modeling to create a reference model for each of the geometries mentioned above. Next, we introduced a new indicator of MEES





Accepted Manuscript For Review Only

efficiency linked to charge distribution: Null material. This indicator defines the proportion of the electrode materials keep inert during charge/discharge cycles. We used the stacked geometry model to explore the effects of the electrode physical parameters (electronic conductivity, ion diffusion coefficient, thickness…) on MEES performance in terms of Null material. Finally, we investigate the charge distribution in our planar model, based on results obtained in the stacked model. We mainly studied the effects of 3D micro-architectured scaffold addition on the charge distribution in the electrode. We also demonstrated that the ionic conductivity of the electrolyte, which was not a limiting factor in the stacked structures, takes a significant role in the planar structures.

Accepted Manuscript
For Review Only

## Results and discussion

**Miniaturized Electrochemical Energy Storage geometry and materials.** There is no consensus on the definition of a MEES. For this study, we used the definition as follow: MEES is a miniaturized device that stores energy through an electrochemical process, such as ion adsorption, metal electrodeposition, or ion intercalation in a matrix. Where at least one of its dimensions is in the range of tens of micrometers or less. For regular MEES, the total footprint area is in the square millimeter range, with exceptional design ranging in the square centimeter range. The typical device is composed of electrodes a few tens of micrometer thick or arrays of micro/nanostructured templates, with one or more of its dimensions in the micrometer scale.

Upon reviewing the literature on this matter, geometries used in the development of MEES can be categorized into two groups: first one we call planar geometries (**Figure 1. a**) and second one we call stacked ones (**Figure 1. b**). Stacked geometries present a vertically organized configuration, where current collectors, electrodes, and electrolytes are in parallel plans on top of each other. In contrast, planar geometry is a horizontally aligned configuration, and it shows that current collectors and electrodes are in the same plane, side by side, with electrolytes on top.

The most straightforward configuration for stacked designs consists of two flat electrodes separated by an electrolyte, as presented in **Figure 1. a**. One example is the work of Ribeiro *et al.*, [13] on LCO-polymer batteries on flexible substrates in 2016. The problem with this design is that the power of the corresponding device is limited. Indeed, the power density of a MEES is directly related to the contact area between electrodes and electrolyte, while its energy density is related to the electrode volume.[14] An attractive solution to increase the power density is to limit the electrode thickness, but in that case, the energy density is thus reduced. To reach a satisfactory energy density with thin-film electrodes, an exciting option is to improve the specific surface of the MEES by





Accepted Manuscript For Review Only

depositing thin-film materials, on a 3D micro-architectured scaffold. From the fabrication point, the main advantage is using semi-conductor compatible processing technologies, such as photolithography and deep reactive ion etching in microelectronics.[15]

There is only few variety of designs available for increasing the specific surface area of a MEES. One of the first designs to experiment is presented in **Figure 1.a.ii**. It consists of depositing a thick layer of the pristine electrode, digging microstructures in tubes, pillars, or trenches inside it firstly, then flooding the microstructures with electrolyte, depositing a flat counter electrode on top, and finally, the current collector.[16] Later, improved deposition techniques coupled with a broader variety of available materials enabled to coat of a microstructured substrate, usually silicon micro-trench/holes/tubes/pillars (**Figure 1. c**), with an Anode-Electrolyte-Cathode Sandwich conforming the microstructure[2,17–20] (**Figure 1.a.iii**). This approach maximizes the contact surface between electrodes and electrolytes (depending on the scaffold). The nature of this geometry offers the possibility to model the device in one dimension with excellent accuracy. However, the use of this architecture is subject to harder physical requirements, *i.e.*, solid electrolytes. Finally, the stacked MEES presents the better surface efficiency compared to planar MEES, as positive and negative electrodes on top of each other and occupy the same footprint area.

Similar to stacked geometries, the simplest planar model consists of two electrodes side by side on current collectors. These designs, very inefficient, were quickly improved by the spatial arrangement of the electrodes.[21] The most common spatial arrangement is the inter-digitated arrangement shown in **Figure 1. b. i & ii**. It consists in designing two electrodes with numerous fingers per electrode polarity. The electrodes can be deposited on the surface of a substrate by 3D printing as in the work of K. Song *et al.*,[22] and T. wang *et al.*,[23] (**Figure 1. b.i**). A more widely used technique is to dig the microstructure directly into the substrate (**Figure 1.b.ii**). Pillars, tubes, wires,





Accepted Manuscript
For Review Only

and trees are then carved or grown inside interdigitated cavities[2,14,18,24,25] and covered per electrode polarity with positive and negative electrode materials, potentially leading to enlargement factor up to ~50 (1 $mm^2$ footprint area leads to a specific surface of ~50 $mm^2$). Bottom-up nano structuration is also possible by growing nanowires or nanotrees directly on the substrate.[26–28]

The electrode materials usually consist of metal oxides for the cathode and various materials for the anode, including metals, metal oxides, or organic materials. In addition, the electrolytes are often gelled, polymerized, or ceramic materials, to limit the technical constraints of handling liquids. A sample of the various materials found in MEES is shown in Table 1.

Accepted Manuscript
For Review Only

Table 1: Common materials used in MEES

| n° ref | geometry | Positive electrode (cathode) | Electrolyte | Negative electrode (anode) | μ structure |
|---|---|---|---|---|---|
| [7] | Planar | LMO[a] | $LiClO_4$ 1M 1:1 EC:DMC | NiSn | Nano-porosity |
| [29] | Planar | PPyDBS[b] | $LiClO_4$ 1M 1:1 EC:DMC | Graphite | micro-pillars |
| [19] | Stacked | MoS2 | HPE[c] | Graphite | honeycomb |
| [20] | Stacked | LCO[d] | LLTO[e] | LMO | honeycomb |
| [30] | Stacked | LCO | LIPON | Li | Thin film |
| [31] | Stacked | LCO | LIPON | Si | Trench |
| [17] | Stacked | LiFePO | LIPON | Si | micro-pillars |
| [16] | Planar | LTO[f] | $LiClO_4$ 1M 1:1 EC:DMC | LFP | Thick film |
| [22] | Stacked | LCO | LIPON | Li | Thin film |
| [32] | Stacked | $MnO_2$ | LIPON | Li | Thin film |
| [32] | Stacked | Zn | LIPON | $MnO_2$ | Thin film |
| [33] | Stacked | $V_2O_5$ | $LiClO_4$ 1M PC | Graphite | Nano-porosity |
| [34] | Stacked | LCO | LIPON | Si | Nano-wire |
| [35] | Stacked | $CF_x$ | $LiPF_6$ PVdF-HFP 1:2 EC:PC | LTO | Thin film |
| [35] | Stacked | SVO[g] | $LiPF_6$ PVdF-HFP 1:2 EC:PC | $TiO_2$ | Thin film |
| [36] | Stacked | LTO | LiTFSI 0.5 M MA-PEG[h] | LNMO[i] | micro-pillars |
| [37] | Planar | LCO | $LiPF_6$ 1M 1:1 EC:DMC | LTO | Thin film |
| [38] | Planar | MPG[j] | $H_3PO_4$/PVA | $MnO_2$ | Meso-porosity |
| [39] | Planar | $RuO_2$ | $H_2SO_4$ | $RuO_2$ | Micro-pillars |
| [40] | Planar | $MnO_2$ | LiCL - PVA | PPy | Nano-porosity |

[a] Lithium Manganese Oxide
[b] Dodecyl-Benzene Sulfonate doped Poly Pyrrole
[c] Hybrid Polymer Electrode
[d] Lithium Cobalt Oxide
[e] Lithium Lanthanum Titanate
[f] Lithium Titanate
[g] Silver Vanadium Oxide
[h] Methyl ether methAcrylate PolyEthylene Glycol
[i] Lithium Nickel Manganese Oxide
[j] Mesoporous Gold

Accepted Manuscript
For Review Only

**Modeling ionic transport in MEES.** COMSOL Multiphysics® is a Finite Element Method (FEM) software designed for "multiphysics": the incorporation and coupling of diverse physical phenomena, expressed as Partial Derivative Equations (PDEs), within one model. Studied phenomena often originate from traditionally separated fields of applied physics and engineering. One electrochemical example of a "multiphysics" problem is battery systems, that often combine mass transport, heat transfer, and charge transfer. Multiphysics simulation can maximize physical insight and accuracy of prediction for a model, as they accurately describe all aspects of a problem.

Comsol Multiphysics® uses a node architecture where PDE relevant to the problem is implemented as "Physics." "Physics" are pre-built interfaces where relevant equations to the physical phenomenon described in the "Physics" are stored and associated with boundaries and domains. Different "Physics" can be coupled together to account for the complexity of the problem. For example, we use "Li-ion battery" coupled with "transport of diluted species" physics in our simulations.

All the models presented in this work are built on COMSOL multiphysics 5.6. Models used classical material: LCO as the positive electrode, graphite as the negative electrode. The electrolyte used for the simulation depends on the geometry previously described. A polymer electrolyte: 1 M $LiPF_6$ EC: DMC 1:2, p(VdF-HFP) is used for planar structures, and LIPON is considered the electrolyte for stacked structures. Materials are based on classically described in the literature and are available in the COMSOL material library. Electrodes are considered non-porous solid with constant volume with lithium insertion (equation 1).

$$Li^+ + e^- + \Theta_s \Leftrightarrow Li\Theta_s \quad (1)$$

$$C_{\Theta_s} = C_{s,max} - C_s \quad (2)$$





Accepted Manuscript For Review Only

With $\Theta_s$ a free reaction site, $Li\Theta_s$ an occupied reaction site at the solid electrode surface, and $C_i$ their concentration.

A trench microbattery was chosen as a classical structure in MEES for stacked geometry.

**Figure 2.** depicts the trench microbattery model in a 3D view. The symmetry along the depth of the model allows for a 2D simplification of the problem (

**Figure 2. b**). The model figures three interdigit units aligned horizontally. One unit comprises a 100 µm long and 10 µm wide digit of the positive electrode, facing an identical digit of the negative electrode and separated by a 1 µm thick electrolyte domain. Both electrode digits are connected to a 10 µm thick horizontal base. This configuration is a little far from what is usually seen for a device built of those materials. Still, we chose to stay close to the configuration reported in the literature for easy comparison.[41] The positive electrode is at the bottom, and the negative electrode is at the top. Finally, a fillet of a 2 µm radius is applied to each internal corner, to smooth the resolution of DPEs and facilitate convergence. Current cycling corresponding to a 1C rate is applied at the positive current collector, and the negative current collector is connected to the ground (

**Figure 2. b**).

The planar geometry features an interdigitated model with planar electrodes buried in cavities. Electrodes are 100 µm wide by 5 µm deep, with 1 µm of electrolyte covering the whole design (

**Figure 2. c**). Alternating positive and negative electrodes align 22 digits, with a gap of 20 µm between each digit. This architecture is based on devices described in Asbani *et al.*[24] and Li *et al.*[42]. The input current is calculated to reach a C-rate = 1 and applied at the bottom of the positive electrode, while the negative electrode is grounded from its bottom. An equivalent stacked model





Accepted Manuscript For Review Only

will be designed to compare planar and stacked architectures. This model will use identical microstructures and same electrolyte, but with a thickness of 10 µm, this value closer to the classical separator thickness for a lithium-ion battery (8 - 30 µm).

The mesh is the second most crucial part of FEM. It defines the location in the model where the PDE are solved. An inadequate mesh will lead to convergence problems, inaccuracy in the model's prediction, and/or overconsumption of computational resources. Automatic Finite Element Mesh is set using the "Physics," "Li-ion Battery," and "Transport of diluted species" as the basis. The mesh is refined along the electrode corner for the trench model to accommodate the expected high gradient at this location.[41] For the planar model, the electrodes were divided into two domains, the upper one at 10% of the depth of the electrode with an excellent mapped mesh, while the rest of the device was meshed using free quads. The model's resolution was then conducted with increasingly finer mesh until the convergence of the values of potential and efficiency. The first mesh with a converging solution comprises 40,702 domain elements and 1 848 boundary elements for the stacked geometry and 158 092 domain elements and 31 886 boundary elements for the planar geometry. The default solver and tolerance proposed by the software were used.

**Mathematical insight of the model.** The mathematical model applied in those simulations is based on the work of Newman and others.[43–47] Equations (3 & (4 are applied in the electrode domains and describe respectively current conservation in the electrode via Kirchhoff's circuit laws and the relationship between current, voltage, and resistance using Ohm's law. Electrodes are considered non-porous solids with sufficient conductivity to prevent the formation of potential gradients. By this hypothesis, we consider that neither convection nor migration occurs. Fick's law of diffusion is then applied to lithium diffusion (equations 5 & 6).

$$\nabla \cdot i_s = Q_s \tag{3}$$





Accepted Manuscript For Review Only

$$i_s = -\sigma_s \nabla \cdot \emptyset_s \quad (4)$$

$$J_i = -D_i \cdot \nabla C_i \quad (5)$$

$$\nabla \cdot J_i = R_i \quad (6)$$

With $i_s$, the current in the electrode ($A$), $Q_s$ an arbitrary current source ($A$), $\sigma_s$ the electrical conductivity in the electrodes ($S$), $\emptyset_s$ the potential in the electrodes ($V$), $J_i$ the flux of matter ($mol.m^{-1}.s^{-1}$), $D_i$ the diffusion coefficient ($m^2.s^{-1}$), $C_i$ the concentration ($mol.m^{-3}$) and $R_i$ the reaction rate ($mol.m^{-1}.s^{-1}$).

In the electrolyte domain, the equations follow concentrated electrolytes theories for conservation of current (equation 7) and mass (equation 8), assuming electroneutrality:

$$\nabla \cdot \left( -\sigma_l \cdot \nabla \phi_l + \frac{2 \cdot \sigma_l \cdot R \cdot T}{F} \left( 1 + \frac{\partial ln(f)}{\partial ln(c_l)} \right) (1 - t_+) \nabla ln(c_l) \right) = i_{tot} + Q_l \quad (7)$$

$$\frac{\partial c_l}{\partial t} + \nabla \cdot (-D_l \cdot \nabla c_l) = R_l - \left( \frac{i_{tot} + Q_l}{F} \right) t_+ \quad (8)$$

With $\sigma_l$ the conductivity of the electrolyte ($S$), $\emptyset_l$ the potential of the electrolyte ($V$), $R$, the gas constant ($J.mol^{-1}.K^{-1}$), $T$, the temperature ($K$), $f$ the activity coefficient, $C_l$, the concentration ($mol.m^{-3}$), $t_+$ the transport number, $i_{tot}$, the current in the electrolyte ($A$) and $Q_l$, arbitrary current source ($A$).

The kinetic at the surface of the electrodes follows the Butler-Volmer relation (equation 9). The current reference density is modified with the state of charge (soc) of the electrode (equation (10 & 11) for an accurate description of lithium insertion.

$$i_{loc,expr} = i_0 \left( exp\left( \frac{\alpha_a F \eta}{RT} \right) - exp\left( \frac{-\alpha_c F \eta}{RT} \right) \right) \quad (9)$$

$$i_0 = i_{0,ref}(T) \left( \frac{c}{c_{s,ref}} \right)^{\alpha_c} \left( \frac{c_{s,max} - c}{c_{s,max} - c_{s,ref}} \right)^{\alpha_a} \left( \frac{c_l}{c_{l,ref}} \right)^{\alpha_a} \quad (10)$$





Accepted Manuscript For Review Only

$$c_{s,ref} = \frac{c_{s,max}}{2} \quad (11)$$

With $i_{0,ref}$, the reference exchange current density ($A.m^{-2}$), $\alpha_a$ and $\alpha_c$ the anodic and cathodic coefficient transfer, $F$, Faraday's constant ($s.A.mol^{-1}$) and $\eta$, the overpotential ($V$) calculated from Nernst equation.

**Null material definition and simulation parameters.** The volume of active material must be uniformly charged if maximum capacity is achieved in electrochemical energy storage systems. To reach this goal, ions must pass from one electrode to another through the electrolyte and then diffuse through the electrode material's entire volume. In a macroscopic system, electrodes typically consist of the electrode material, an electronically conductive additive, and a binder, all in the form of a composite porous matrix. Porous electrodes provide a high contact area between the electrode material and the electrolyte. The small size of the particles (in the order of a few tens nm) and the electrolytes' high ionic conductivity make the electrodes' electrical conductivity the main limiting factor in obtaining a homogeneous charge.[41] However, in a micro-battery, the deposition method of active materials (= thin films) leads to the formation of dense layers. Thus, the electrolyte does not penetrate the electrode, reducing the contact area between the electrolyte and the active material. This work investigates the effect of material properties and the applied Crate (i.e. the current density) on the charge distribution.

The charge heterogeneity in the cell is quantified in terms of Null material Nm. Null material is calculated from equation 12. For simplicity, the cell has been drawn symmetrically, so there is an imbalance between the charge and discharge cycle caused by the higher capacity of the negative electrode. Since the positive electrode is the limiting electrode in the system, the maximum theoretical capacity and current calculations were obtained with its physical and chemical





Accepted Manuscript For Review Only

characteristics. The concentration of lithium in the electrodes allows qualifying graphically the distribution of the charge in the electrode.

$$N_m = 1 - \frac{Q}{Q_{max}} \quad (12)$$

With $N_m$ the fraction of Null material in the cell, $Q$ charge in $A.h$ and $Q_{max}$ the maximum charge in $A.h$.

The different parameters that remain constant for all simulations are given in Table 2. The reference exchange current represents the oxidation and reduction rates for a given single electrode at equilibrium. It is used in the Butler-Volmer equations at both positive and negative electrodes. The charge state is the ratio of the current lithium-ion concentration in the electrode to its theoretical maximum. $C_{rate}$, conductivity, diffusion coefficient, and electrode thickness were tuned independently during the simulation. First, the $C_{rate}$ value was set to C/n for values of n ranging from 0.5 to 3.[48]. Next, the battery's maximum charge capacity is calculated from the material maximum lithium concentration of the limiting electrode (negative electrode here), the electrode's maximum state of charge, the electrode's volume, and the faraday constant. This value is then used to calculate the current associated with each $C_{rates}$. Then, at a reference $C_{rate}$ of 1C, the conductivity of the positive electrode was increased stepwise from its initial value, 1 S/m, to the value of the negative electrode at 100 S/m.[49,50] Following that, the diffusion coefficient in both electrodes varied from its initial value, $10^{-14}$ cm²/s, [51] to its final value of $10^{-6}$ cm²/s. Next, the upper limit value of the diffusion coefficient has been set to reach the minimum $N_m$ achievable for this model. Finally, the electrode thickness varied from 1 µm to 20 µm (not including substrate thickness), which are reasonable thicknesses for MEES.[24,42] The cut-off conditions of the model are based on cell voltage. The cell voltage is calculated from material properties and electrode state of charge. The boundaries involved in the calculus of cell voltage have been highlighted in **Figure 2**. This cut-off condition





Accepted Manuscript For Review Only

has been established on the premise that forced overcharge cause the electrode material and the electrolyte to deteriorate as the cell voltage increase.

Table 2: List and values of the parameters used in the modelization.

| Parameter | Physical significance | value |
|---|---|---|
| $i0_{ref,neg}$ | Reference exchange current density for the negative electrode | 1.72 $A.m^{-2}$ |
| $i0_{ref,pos}$ | Reference exchange current density for positive electrode | 0.96 $A.m^{-2}$ |
| $V_{elec}$ | Electrode volume | 3.67 10-4 $mm^3$ |
| F | Faraday's constant | 96485 $C.mol^{-1}$ |
| $C_{max}$ | Maximum Lithium-ion concentration in graphite electrode | 31507 $mol.L^{-1}$ |
| $SoC_{max}$ | Maximum state of charge for the graphite electrode | 0.98 |
| $Q_{max}$ | Maximum charge capacity of the limiting electrode | 1.0934 $10^{-3}$ C |
| $1C_{current}$ | Charge/discharge current at 1C rate | 3.0371 $10^{-1}$ µA |
| $C_{elec}$ | Initial concentration in the electrolyte | 16 $mol.L^{-1}$ |

**Performance of the stacked trench model at 1C current.** The model was parameterized with a state of charge (soc) of 0.5 as initial conditions. It was then submitted to a 1C discharge current until the cut-off conditions were met, followed by a charge-discharge cycle. Triggers for the charge-discharge are given by the potential difference across the device with maximum and minimum authorized voltage given by the material properties. The charge-discharge curve is given in **Figure 3**. a and matches the shape expected for such a device.[52] As expected, the fraction of Null material of the cell is relatively high (77.3% in charge vs. 75.4% in discharge) even at moderate $C_{rate}$. However, the difference mentioned above in Null material between charge and discharge comes from the initial condition and would disappear over sufficient cycling. Therefore, it has been deemed negligible as the calculated charge and discharge Null material difference is about 1.9%. In addition, the computational resources required to stabilize the system and perfectly equalize the charge and discharge of Null material are quite large. Thus, from this point on, the average Null material between the charge cycle and the discharge cycle will be used in this report as an acceptable approximation.

Accepted Manuscript
For Review Only

The monitoring of the heterogeneity of the charge in the electrodes is done by direct observation of the state of charge (soc) in the model electrodes. **Figure 3. b** shows a representation of this concentration at various characteristic moments of the cell simulation with the original material characteristics and a charge/discharge rate of 1C. In the initial state, **Figure 3. b.o**, the lithium concentrations in the positive and negative electrodes are given for 50% of their maximum concentrations.

Soc is homogeneous in the positive electrode during the whole charge/discharge cycle with a value between 0.75 when the system is discharged and 0.5 when the system is charged. At the beginning of the charge (**Figure 3. b.i**), the negative electrode shows heterogeneity of charge between the digit (A), where the soc is about 0.2, and the base (B), where the soc is about 0.5. The digit presents charge heterogeneity with a surface close to a soc of 0 and a center of the digit with a soc close to 0.3. The negative electrode base also presents charge heterogeneity with a soc close to 0.2 near the electrolyte and a soc about 0.4 deeper in the electrode. During charge (**Figure 3.b.ii**), the negative electrode presents two zones where soc is homogeneous. The digit part of the electrode (A) with a soc of about 0.3 and the base (B) with a soc of about 0.5. At the end of the charge (**Figure 3.b.iii**), the negative electrode digit (A) presents a strong gradient of soc with the surface soc about 0.7 and a soc about 0.2 deeper in the electrode digit. The electrode base (B) is more homogeneous with about 0.5. During discharge (Figure 3**.b.iv**), the negative electrode digit (A) presents a homogeneous soc of about 0.3. While going closer to the base (B), a soc gradient appears with soc about 0.3 at the surface and soc about 0.5 deeper in the electrode. At the end of discharge (**Figure 3. b.v**), the soc in the negative electrode is back to the beginning of the charge (**Figure 3. b.i**). As we see with the gradient of Lithium-ion in the electrodes, the top of the graphite electrode barely participates in the charge-discharge process. This inactive volume of electrode material is the null





Accepted Manuscript
For Review Only

material in the device. The heterogeneity in the soc in positive and negative electrodes can be assigned to two factors: diffusion coefficient and electronic conductivity. The diffusion coefficient of lithium ions in the positive electrode is 5 times greater than in the negative electrode. This difference explains that the soc is more homogeneous inside the positive electrode than inside the negative electrode.

**The electrical conductivity of the electrode is not a limiting factor.** Electrical conductivity has been suggested as a potential cause of charge heterogeneity in electrochemical energy storage systems. However, as demonstrated in the present study, the electrodes' location and intensity of state of charge heterogeneity do not fit this assignment.

The fraction of Null material varies only slightly when the conductivity of the positive electrode increases going from 70.6% of Null material at the initial conductivity of 1 S/m to 69.76% at a conductivity of 100 S/m corresponds to that of the negative electrode conductivity. It has been shown that charge heterogeneity at the end of digital structures is expected and has been partially assigned to the difference in conductivity between the electrodes and the geometry of the structure (size of the digits and curvature radius of the digit top). However, the contribution of the electrical conductivity difference in the model is limited to a few percentiles of the total charge heterogeneity. This suggests more impactful phenomena than the conductivity discrepancy between the electrodes that generate charge heterogeneity in 3D-MBs.

**The diffusion coefficient is the limiting factor in MEES design.** Apart from the charge difference that can be assigned to the difference in electrical conductivity between the electrodes, an analysis of equations 4 et 5 suggests that the phenomenon at the origin of most of the charge heterogeneity in the present model comes from diffusion lithium-ion in the electrodes. The diffusion coefficient of lithium in the electrodes was equalized between the two electrodes before varying it from $10^{-20}$





Accepted Manuscript For Review Only

m²/s to $10^{-9}$ m²/s, respectively the most minor and most incredible values for state-of-the-art electrode materials.

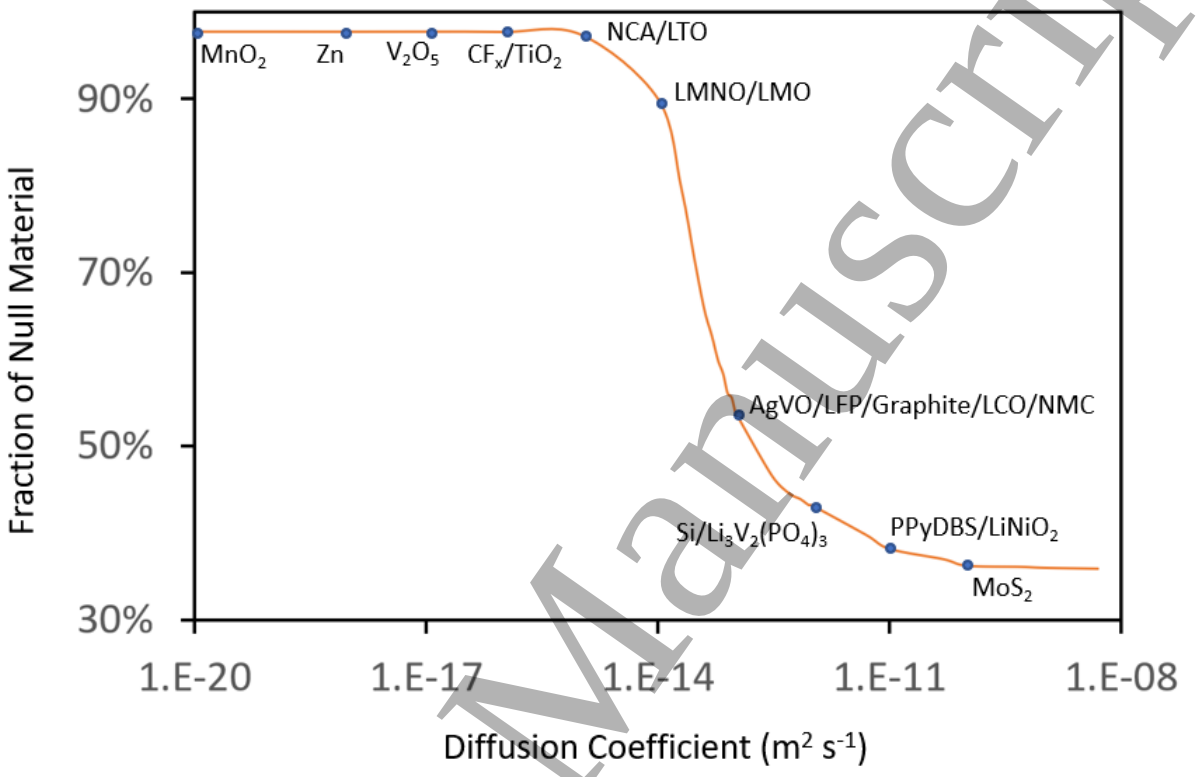


**Figure 4** shows the variation of the fraction of Null material and thus the heterogeneity generated as a function of the diffusion coefficient of lithium-ion in the electrodes.

Accepted Manuscript

The curve can be split into three different zones. The first zone (

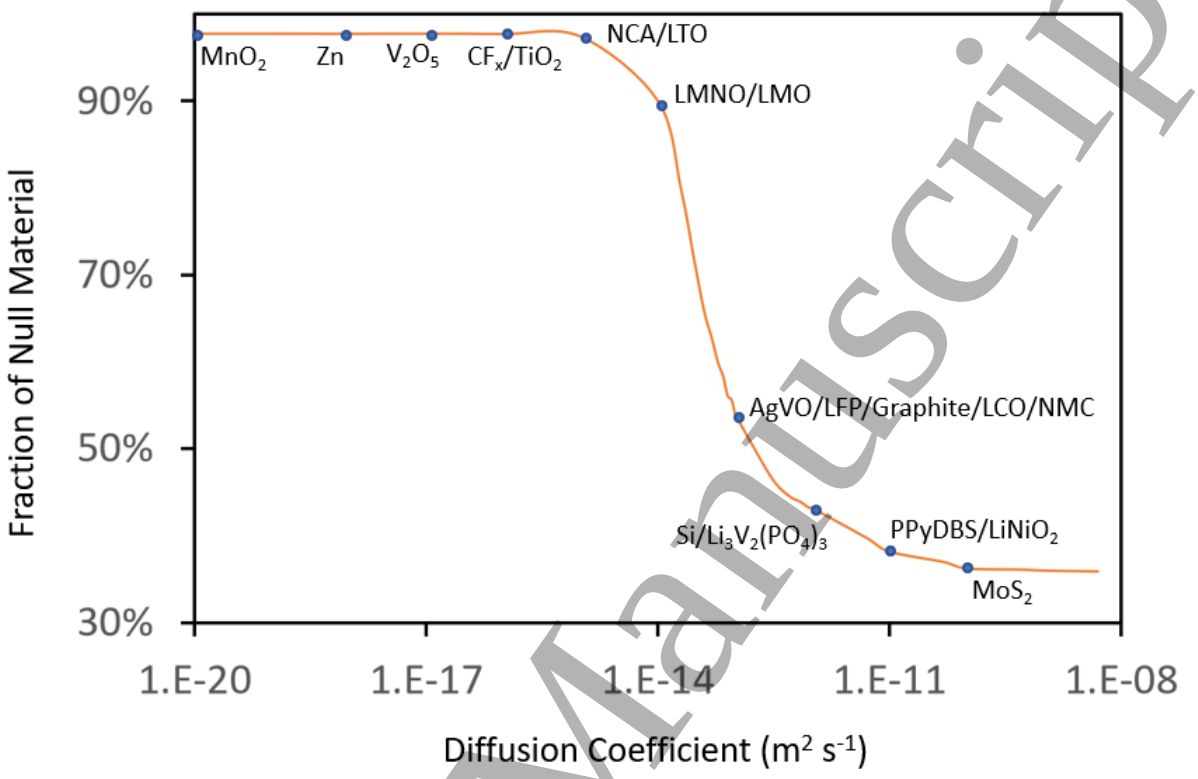


**Figure 4. c**) corresponds to a diffusion coefficient between $10^{-20}$ to $10^{-15}$ $m^2$ $s^{-1}$. In this zone, the fraction of Null material is constant at about 98%. The second zone (

Accepted Manuscript
For Review Only

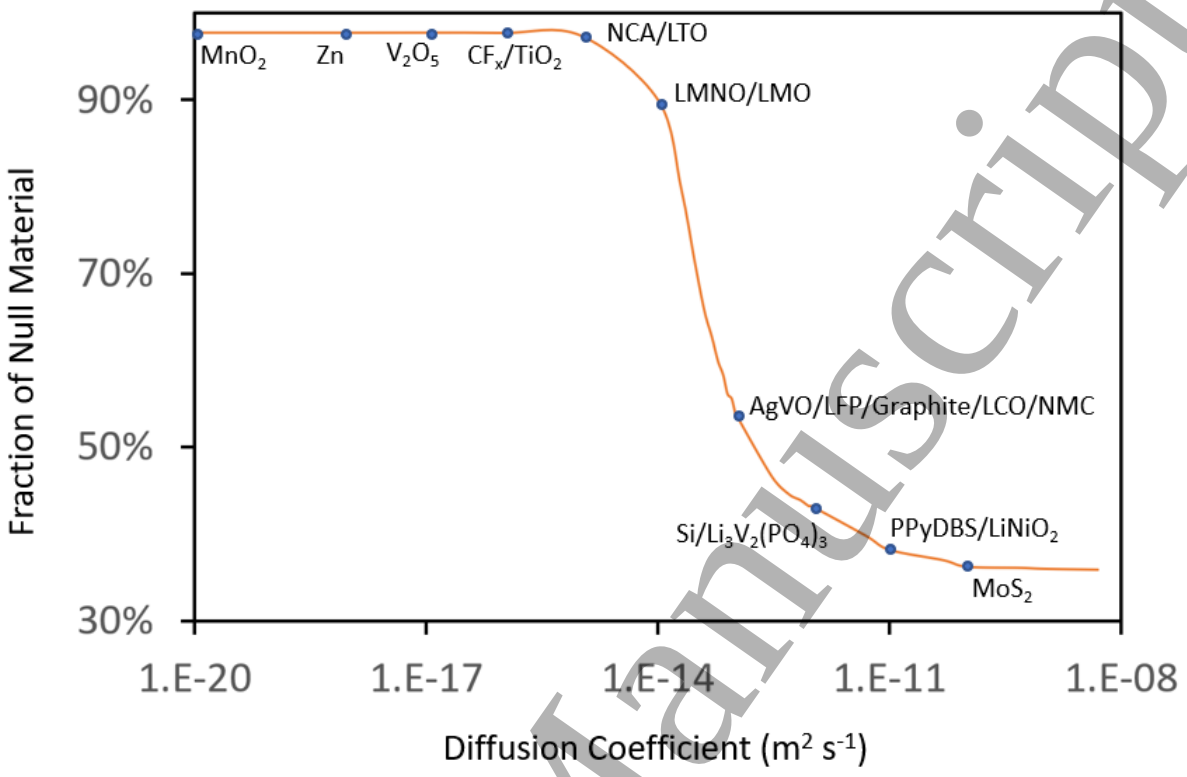


**Figure 4. a & b**) sees the fraction of Null material dropping rapidly from 98 to 50% of Null material for diffusion coefficient between $10^{-15}$ and 2 $10^{-13}$ $m^2$ $s^{-1}$. Then the fraction of Null material gently decreases to 38% for diffusion coefficient up to $10^{-11}$ $m^2$ $s^{-1}$. The third zone (

Accepted Manuscript
View Only

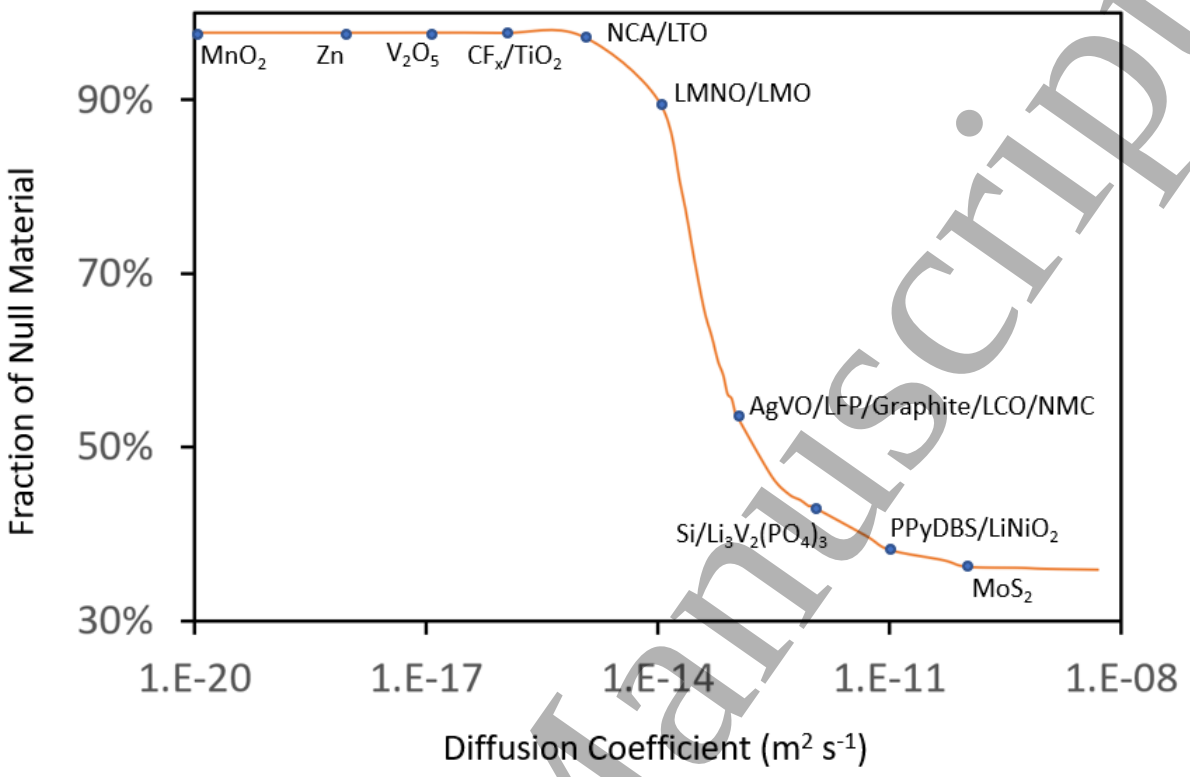


**Figure 4.b**) is a plateau where the fraction of Null material stays constant at a value about 36% for diffusion coefficients lower than 2 $10^{-11}$ $m^2$ $s^{-1}$. It follows that most of the charge heterogeneity in the cell comes from the difficulty of lithium ions to diffuse throughout the electrodes. Since modifying the diffusion coefficient of lithium in the electrodes is practically impossible, it becomes obvious that monitoring the microstructure thickness is the first factor of improvement for miniaturized electrochemical energy storage systems.

**Tuning charge factor and electrode thickness to decrease charge heterogeneity.** An alternative way to decrease charge heterogeneity and thus increase the storage efficiency is to play on the charge-discharge rate. Equation 3 indicates that giving more time to lithium ions to diffuse allows them to sink deeper into the microstructures and therefore decreases the impact of the diffusion coefficient on the charge heterogeneity. **Figure 5.a** shows the variation of the charge storage efficiency as a function of the charge/discharge rate applied to the cell.





Accepted Manuscript
View Only

As with diffusion coefficient, changing the charge/discharge rate does not have a linear effect on the charge heterogeneity, which is consistent with Equations 1, 6, and 7.

The model shows that a 3C rate is already well beyond the capacity of the presented microstructures since only 0.6% of the active material is involved. This value increases to 2.2% for a 2C rate and then to 26.7% when the rate increases to 1C. At 0.5C, the fraction of Null material is below 50%. At slower rate, the observed gain in efficiency is less and less as the rate of charge/discharge slows down. Projections show that the fraction of Null material should reach a plateau of about 13%. This further confirms that the limitation in the miniaturized electrochemical energy storage lies mostly in the diffusion of ions in the electrodes.

As expected, the charge-discharge rate used to operate an electrochemical energy storage system has a dominant impact on the charge heterogeneity in the electrodes. In this way, it is a major parameter to be taken into account in the elaboration of microstructures for electrochemical energy storage.

Similarly, the thickness of the electrodes is related to the creation of charge heterogeneity in the MEES. Indeed, the thicker the electrode, the deeper the lithium ions have to diffuse into the electrode for a full charge. However, a thinner electrode would contain less material and would therefore be able to store less energy (but more efficiently). The thickness of the electrode and electrolyte have been varied from 1 µm which is a typical thickness for thin film depicted in literature,[19] to 20 µm which is an average thickness for MEES[53].

**Figure 5.b** depicts the fraction of Null material in the system as vs the thickness of the electrodes at 1C. As presented on the graph, the fraction of Null material in the electrode follows a linear curve with a constant increase of the Null material fraction in the system followed by a plateau at about 15 µm electrode thickness and above.





Accepted Manuscript
For Review Only

**Charge heterogeneity in electrode and electrolyte for same plane geometry.** Like the stacked model, the planar models have been parameterized with a state of charge corresponding to 50% of the maximum charge in each electrode. Electrodes were then fully discharged at 1C followed by charge-discharge cycles. The charge/discharge thresholds are given by the minimum and maximum voltage allowed, derived from the material properties. The number of digit pairs were increased stepwise to 20 pairs of digits. After 10 pairs of digits, the edge effects become negligible to the point that the fraction of Null material in the system becomes constant at a value of 82.69%.

As can be seen in **Figure 6**, the charge-discharge profile is modified by the interdigitated system arrangement compared to the stacked arrangement. The electrochemical window used in the model has been shifted by 0.2 V towards the higher potentials, which facilitates the convergence of the simulation. As expected, the fraction of Null material in the planar model is also greater than in a stacked model of equivalent thickness (82.69% versus 73.3%). The lithium concentration gradient in the electrolyte in a stacked model is small, ranging over 0.04 $mol.L^{-1}$ from minimum to maximum concentrations. The gradient is parallel to the electrode surfaces (**Figure 7.a**). It allows the surface of the electrode to be homogeneously affected upon charge and discharge cycling. In contrast, the lithium concentration gradient in the electrolyte in a planar model is more marked, ranging over 1 $mol.L^{-1}$ from minimum to maximum concentrations. The gradient is also oriented perpendicular to the electrode surfaces (**Figure 7.b**). This makes the rate of electrode mobilization heterogeneous[41] with maxima located on the sides of the electrode, near the gap between the digits. This is a consequence of the ionic pathway between the two electrodes in the various configurations. The profiles of electrode soc confirm this point with a state of charge greater on edges, close to the surface of the electrode compared to the center and the depth of the electrode (**Figure 7.c**).

Accepted Manuscript
For Review Only

The addition of micro-architectured scaffold in the planar system further complicates the ionic pathway to the electrode surface compared to a stacked system. This complex ionic pathway of lithium ion first in between the microstructures, then between the two electrodes induces an heterogeneity in the electrode surface mobilization, even greater than in the case of 2D microelectrodes. The gap between the minimum and maximum values of the lithium concentration reaches 2.4 $mol.L^{-1}$ (**Figure 7.c**). The maximum and minimum concentrations are located in between the central microstructures of the positive and negative electrode, respectively.

This is a result of three factors: the transfer kinetics of lithium ions from the electrode to the electrolyte the diffusion of ions within the electrolyte and finally the diffusion of ions within the electrodes. The electrolyte reaches almost zero lithium-ion concentration between the microstructures during charge/discharge. Similarly, at the opposite electrode, the lithium ion concentration reaches 2.5 $mol.L^{-1}$. These differences in concentrations can induce some problems of structural nature, chemical nature or solubility depending on the chosen electrolyte.

Similarly, the thin gap between the two electrodes is a potential limitation to be accounted for in the design of a micro-battery. This passage is indeed the only bridge connecting the positive and negative electrodes. It will allow all the lithium ions involved in the charge/discharge of the cell to pass through. Therefore, the current density in the electrolyte will be maximum at this specific location.

**Conclusion**

This work investigated the limiting factors driving the MEES efficiency by defining a new indicator: the fraction of Null material in the cell. It corrected some misleading assumptions about MEES limitation by demonstrating that contrary to previous claims, the electrical conductivity, and the difference in electrical conductivity between positive and negative electrodes, do not cause any





Accepted Manuscript For Review Only

significant loss of efficiency in the device. It has also demonstrated the predominant role of ionic diffusion in the electrodes with respect to charge heterogeneity in MEES. A low ionic conductivity must be associated with a low $C_{rate}$, to limit charge heterogeneity in a device and thus increase storage efficiency. With an exponential growth of Null material with the $C_{rate}$, the charge applied to the cell is the most critical factor to consider when designing a MEES.

Furthermore, several limitations concerning the electrolyte and architecture have arisen at the mesoscale level. The ionic pathway has been identified as a potential weak point in the design of efficient MEES. Further work is needed to quantify and qualify the ionic pathway effects through the microstructures and the different architectures.

This work finally serves as a basement for further work, to determine the accurate relationship between geometry, diffusion coefficient and $C_{rate}$ applied for maximizing energy storage efficiency. More investigation on realistic 3D structures should follow using the knowledge currently gained to build more efficient cells. The insight gained will help to associate each material and use within an efficient geometry.

**Acknowledgement**

This research is financially supported by the ANR within the DENSSCAPIO project (ANR-17-CE05-0015-02). The authors also want to thank the ANR STORE-EX and the French network on electrochemical energy storage (RS2E) for the financial support. The French RENATECH network is greatly acknowledged for the use of microfabrication facilities.

Accepted Manuscript
For Review Only

## Bibliography


[1] Cao, D.; Xing, Y.; Tantratian, K.; Wang, X.; Ma, Y.; Mukhopadhyay, A.; Cheng, Z.; Zhang, Q.; Jiao, Y.; Chen, L.; Zhu, H. **2019** *Adv. Mater. 31*, 1–10.

[2] Létiche, M.; Eustache, E.; Freixas, J.; Demortière, A.; De Andrade, V.; Morgenroth, L.; Tilmant, P.; Vaurette, F.; Troadec, D.; Roussel, P.; Brousse, T.; Lethien, C. **2017** *Adv. Energy Mater. 7*, 1–12.

[3] Javed, M. S.; Lei, H.; Shah, H. U.; Asim, S.; Raza, R.; Mai, W. **2019** *J. Mater. Chem. A 7*, 24543–24556.

[4] Wu, X.; Huang, B.; Lv, R.; Wang, Q.; Wang, Y. **2019** *Chem. Eng. J. 378*, 122246.

[5] El-Kady, M. F.; Kaner, R. B. **2013** *Nat. Commun. 4*, 1475–1479.

[6] Yun, J.; Lee, H.; Song, C.; Jeong, Y. R.; Park, J. W.; Lee, J. H.; Kim, D. S.; Keum, K.; Kim, M. S.; Jin, S. W.; Lee, Y. H.; Kim, J. W.; Zi, G.; Ha, J. S. **2020** *Chem. Eng. J. 387*, 124076.

[7] Pikul, J. H.; Gang Zhang, H.; Cho, J.; Braun, P. V.; King, W. P. **2013** *Nat. Commun. 4*, 1–5.

[8] Delannoy, P. E.; Riou, B.; Lestriez, B.; Guyomard, D.; Brousse, T.; Le Bideau, J. **2015** *J. Power Sources 274*, 1085–1090.

[9] Wang, Z.; Ni, J.; Li, L.; Lu, J. **2020** *Cell Reports Phys. Sci. 1*, 100078.

[10] Arico, C.; Ouendi, S.; Taberna, P. L.; Roussel, P.; Simon, P.; Lethien, C. **2019** *ACS Nano 13*, 5826–5832.

[11] Miyamoto, K.; Sasaki, T.; Nishi, T.; Itou, Y.; Takechi, K. **2020** *iScience 23*, 101317.

[12] Li, Y.; Qu, J.; Li, F.; Qu, Z.; Tang, H.; Liu, L.; Zhu, M.; Schmidt, O. G. **2021** *Nano Mater.*


Accepted Manuscript
For Review Only

*Sci. 3*, 140–153.

[13] Ribeiro, J. F.; Sousa, R.; Vieira, E. M. F.; Rolo, A. G.; Silva, M. M.; Dupont, L.; Correia, J. H.; Goncalves, L. M. **2016** *J. Mater. Sci. Mater. Electron. 27*, 631–636.

[14] Lethien, C.; Le Bideau, J.; Brousse, T. **2019** *Energy Environ. Sci. 12*, 96–115.

[15] Pimpin, A.; Srituravanich, W. **2012** *Eng. J. 16*, 37–55.

[16] Lethien, C.; Zegaoui, M.; Roussel, P.; Tilmant, P.; Rolland, N.; Rolland, P. A. **2011** *Microelectron. Eng. 88*, 3172–3177.

[17] Baggetto, L.; Niessen, R. A. H.; Roozehoom, F.; Notten, P. H. L. **2008** *Adv. Funct. Mater. 18*, 1057–1066.

[18] Eustache, E.; Tilmant, P.; Morgenroth, L.; Roussel, P.; Patriarche, G.; Troadec, D.; Rolland, N.; Brousse, T.; Lethien, C. **2014** *Adv. Energy Mater. 4*, 1–11.

[19] Nathan, M.; Golodnitsky, D.; Yufit, V.; Strauss, E.; Ripenbein, T.; Shechtman, I.; Menkin, S.; Peled, E. **2005** *J. Microelectromechanical Syst. 14*, 879–885.

[20] Kotobuki, M.; Suzuki, Y.; Munakata, H.; Kanamura, K.; Sato, Y.; Yamamoto, K.; Yoshida, T. **2010** *J. Electrochem. Soc. 157*, A493.

[21] Liu, N.; Gao, Y. **2017** *Small 13*, 1–10.

[22] Sun, K.; Wei, T. S.; Ahn, B. Y.; Seo, J. Y.; Dillon, S. J.; Lewis, J. A. **2013** *Adv. Mater. 25*, 4539–4543.

[23] Wang, T.; Li, L.; Tian, X.; Jin, H.; Tang, K.; Hou, S.; Zhou, H.; Yu, X. **2019** *Electrochim. Acta 319*, 245–252.

[24] Asbani, B.; Bounor, B.; Robert, K.; Douard, C.; Athouël, L.; Lethien, C.; Le Bideau, J.;





Accepted Manuscript For Review Only

Brousse, T. **2020** *J. Electrochem. Soc. 167*, 100551.

[25] Asbani, B.; Buvat, G.; Freixas, J.; Huvé, M.; Troadec, D.; Roussel, P.; Brousse, T.; Lethien, C. **2021** *Energy Storage Mater. 42*, 259–267.

[26] Gentile, P.; Solanki, A.; Pauc, N.; Oehler, F.; Salem, B.; Rosaz, G.; Baron, T.; Den Hertog, M.; Calvo, V. **2012** *Nanotechnology 23*.

[27] Oehler, F.; Gentile, P.; Baron, T.; Ferret, P.; Den Hertog, M.; Rouvière, J. **2010** *Nano Lett. 10*, 2335–2341.

[28] Gaboriau, D.; Aradilla, D.; Brachet, M.; Le Bideau, J.; Brousse, T.; Bidan, G.; Gentile, P.; Sadki, S. **2016** *RSC Adv. 6*, 81017–81027.

[29] Min, H. S.; Park, B. Y.; Taherabadi, L.; Wang, C.; Yeh, Y.; Zaouk, R.; Madou, M. J.; Dunn, B. **2008** *J. Power Sources 178*, 795–800.

[30] Grillon, N.; Bouyssou, E.; Jacques, S.; Gautier, G. **2015** *J. Electrochem. Soc. 162*, A2847–A2853.

[31] Oudenhoven, J. F. M.; Baggetto, L.; Notten, P. H. L. **2011** *Adv. Energy Mater. 1*, 10–33.

[32] Ferrari, S.; Loveridge, M.; Beattie, S. D.; Jahn, M.; Dashwood, R. J.; Bhagat, R. **2015** *J. Power Sources 286*, 25–46.

[33] Ergang, N. S.; Fierke, M. A.; Wang, Z.; Smyrl, W. H.; Stein, A. **2007** *J. Electrochem. Soc. 154*, A1135.

[34] Ruzmetov, D.; Oleshko, V. P.; Haney, P. M.; Lezec, H. J.; Karki, K.; Baloch, K. H.; Agrawal, A. K.; Davydov, A. V.; Krylyuk, S.; Liu, Y.; Huang, J.; Tanase, M.; Cumings, J.; Talin, A. A. **2012** *Nano Lett. 12*, 505–511.

Accepted Manuscript
For Review Only

[35] Wang, Y.; Liu, B.; Li, Q.; Cartmell, S.; Ferrara, S.; Daniel, Z.; Xiao, J. **2015** *J. Power Sources 286*, 330–345.

[36] Nasreldin, M.; Delattre, R.; Calmes, C.; Ramuz, M.; Sugiawati, V. A.; Maria, S.; Tocnaye, J. L. de B. de la; Djenizian, T. **2020** *Energy Storage Mater. 33*, 108–115.

[37] Hoeppner, K.; Ferch, M.; Froebe, A.; Gernhardt, R.; Hahn, R.; Mackowiak, P.; Mukhopadhyay, B.; Roder, S.; Saalhofen, I.; Lang, K. D. **2015** *J. Phys. Conf. Ser. 660*, 3–8.

[38] Xia, F.; Xu, S.; Gao, Q.; Wang, X. **2020** *Proc. IEEE Int. Conf. Micro Electro Mech. Syst. 2020-Janua*, 614–617.

[39] Liu, C. C.; Tsai, D. S.; Susanti, D.; Yeh, W. C.; Huang, Y. S.; Liu, F. J. **2010** *Electrochim. Acta 55*, 5768–5774.

[40] Zhang, C.; Xiao, J.; Qian, L.; Yuan, S.; Wang, S.; Lei, P. **2016** *J. Mater. Chem. A 4*, 9502–9510.

[41] Zadin, V.; Brandell, D.; Kasemägi, H.; Aabloo, A.; Thomas, J. O. **2011** *Solid State Ionics 192*, 279–283.

[42] Li, S.; Wang, X.; Shen, C.; Wang, J.; Kang, F. **2012** *Micro Nano Lett. 7*, 744–748.

[43] Thomas, K.; Newman, J.; Darling, R. **2000** *Electrochim. Acta 45*, 2595–2609.

[44] Doyle, M.; Fuller, T. F.; Newman, J. **1993** *J. Electrochem. Soc. 140*, 1526–1533.

[45] Doyle, M.; Newman, J. **1995** *J. Power Sources 54*, 46–51.

[46] Christensen, J.; Newman, J. **2003** *Proc. - Electrochem. Soc. 20*, 85–94.

[47] Fuller, T. F.; Doyle, M.; Newman, J. **1994** *J. Electrochem. Soc. 141*, 1–10.

Accepted Manuscript
For Review Only

[48] Lee, S. J.; Lee, C. Y.; Chung, M. Y.; Chen, Y. H.; Han, K. C.; Liu, C. K.; Yu, W. C.; Chang, Y. M. **2013** *Int. J. Electrochem. Sci. 8*, 4131–4141.

[49] Tian, R.; Park, S. H.; King, P. J.; Cunningham, G.; Coelho, J.; Nicolosi, V.; Coleman, J. N. **2019** *Nat. Commun. 10*.

[50] Tian, R.; Alcala, N.; O'Neill, S. J. K.; Horvath, D. V.; Coelho, J.; Griffin, A. J.; Zhang, Y.; Nicolosi, V.; O'Dwyer, C.; Coleman, J. N. **2020** *ACS Appl. Energy Mater. 3*, 2966–2974.

[51] Liu, W.; Shi, Q.; Qu, Q.; Gao, T.; Zhu, G.; Shao, J.; Zheng, H. **2017** *J. Mater. Chem. A 5*, 145–154.

[52] Jeon, Y.; Noh, H. K.; Song, H. K. **2017** *Sci. Rep. 7*, 1–10.

[53] Kyerematen, N. A.; Brousse, T.; Pech, D. **2017** *Nat. Nanotechnol. 12*, 7–15.

[54] Eustache, E.; Douard, C.; Demortière, A.; De Andrade, V.; Brachet, M.; Le Bideau, J.; Brousse, T.; Lethien, C. **2017** *Adv. Mater. Technol. 2*, 1700126.

Accepted Manuscript
For Review Only

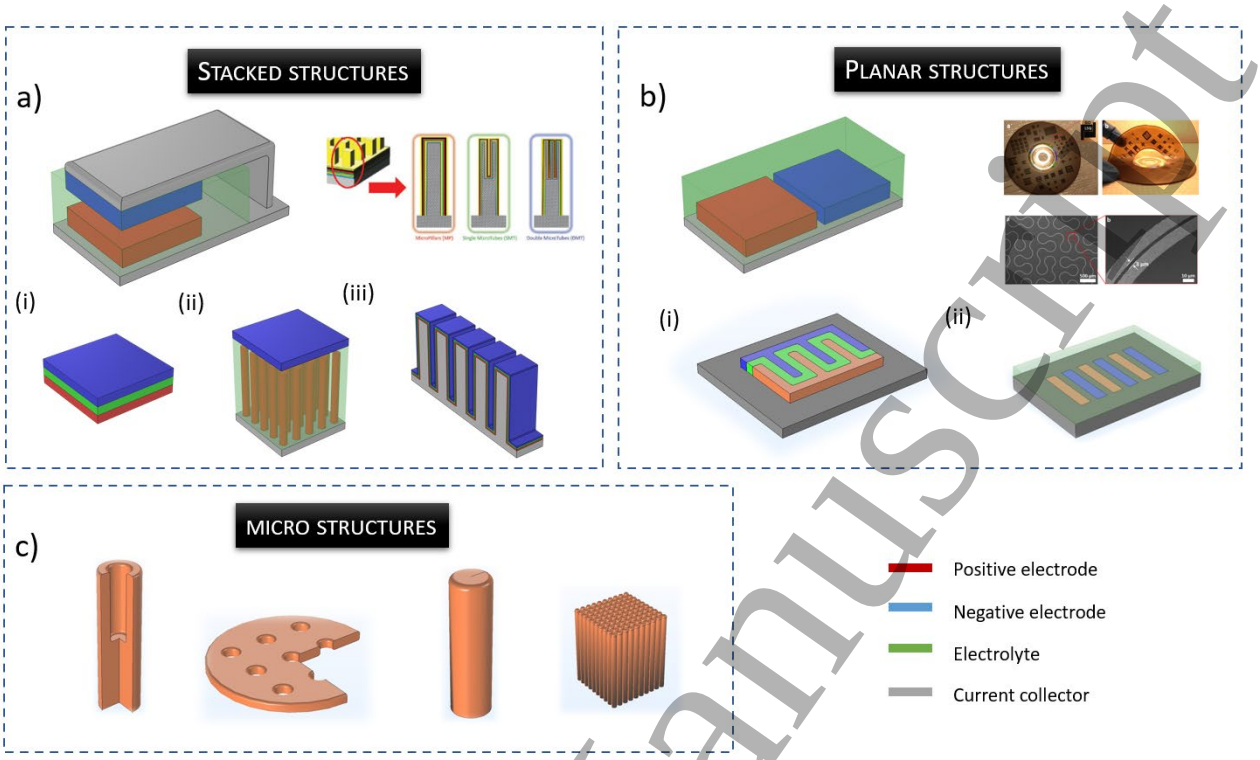


**Figure 1: Schematic of the different MEES architectures and microstructures. (a)** Stacked geometry with a schematic diagram at the top left and its application by Létiche *et al,*.[2] **(i)** Schematic of a simple stacked structure, **(ii)** a semi-structured stacked structure and **(iii)** a fully microstructured stacked structure. **(b)** Planar geometry with a schematic diagram at the top left and two applications by et El-Kady *et al,*[5] and Yun *et al,*[6] at the top right. **(i)** schematic of a planar interdigitated structure deposited on a substrate and **(ii)** schematic of a planar interdigitated structure in cavity.[54] **(c)** Most common microstructures used to increase the specific surface of electrodes with, from left to right, a micro-tube, a micro-perforated structure, a micro-pillar and nanowires.

Accepted Manuscript
For Review Only

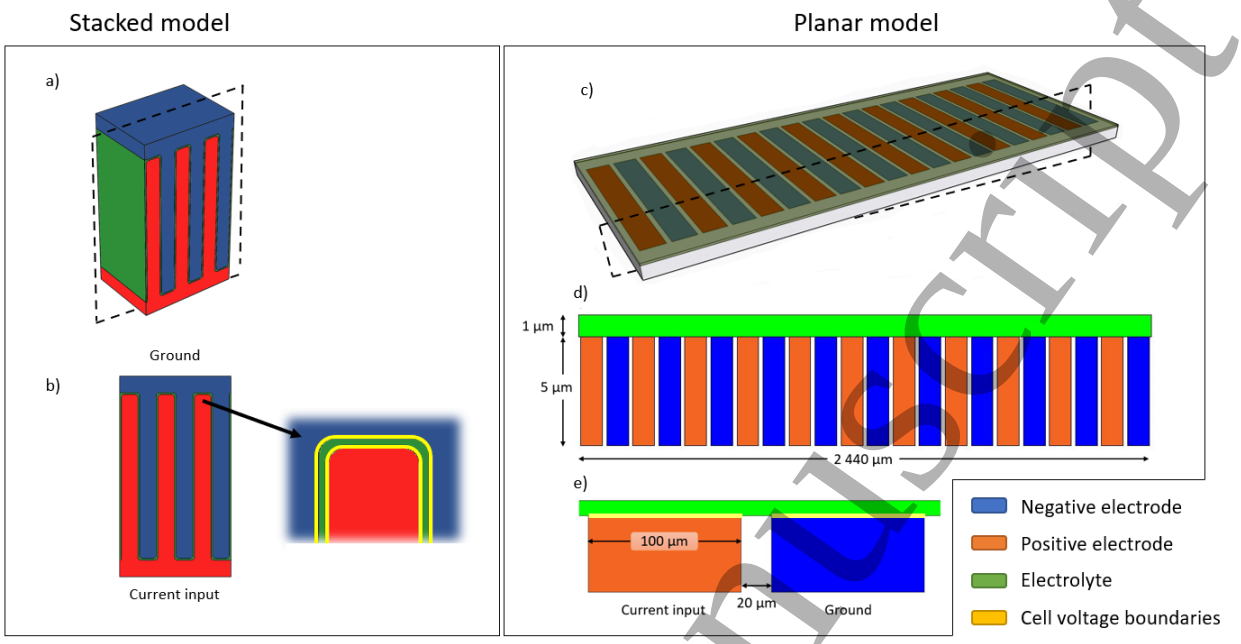


**Figure 2**: **Reference model for stacked (a & b) and planar (c & d) geometries. (a)** 3-dimension trench model and **(b)** corresponding 2-dimension model used in the first part of the study. Current is injected at the bottom of the positive electrode and sink at the top of the negative electrode. **(c)** 3-dimension view of the planar interdigit thick film burried in cavities model. **(d)** corresponding 2-dimention model used in the second part of the study. Current is injected at the bottom of the positive digits and sink at the bottom of the négative digits. The model is represented at a 1 to 50 (horizontal-vertical) ratio for the complete model and **(e)** at a 1 to 10 ratio for a single pair of digit. In both models, Negative electrode are figure in blue, positive electrode in red, surfaces used for cell voltage calculation in yellow and electrolyte in green.

Accepted Manuscript
Review Only

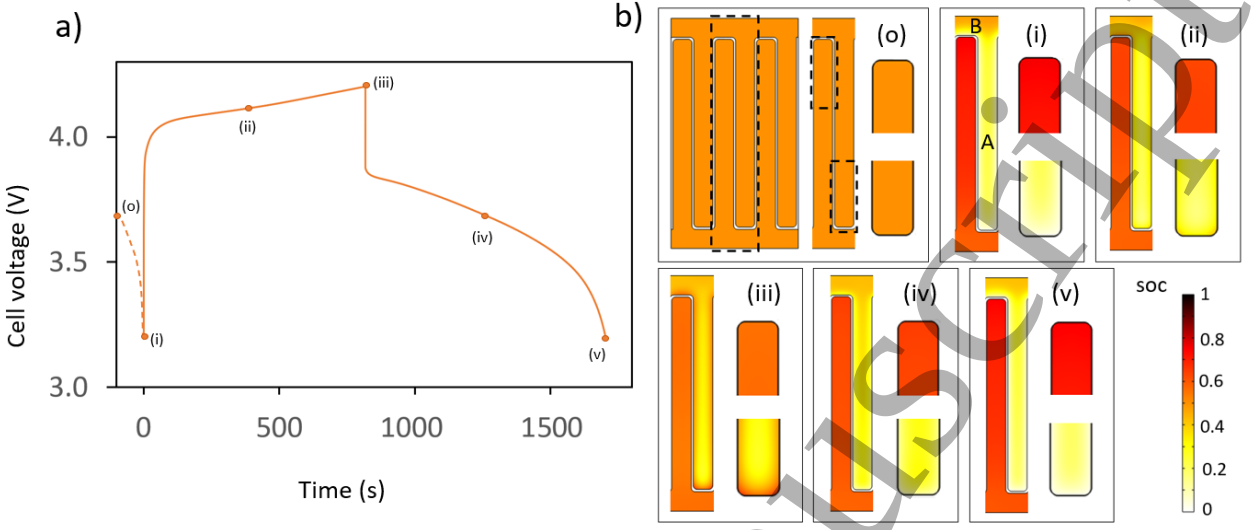


**Figure 3: Simulated battery performance for the graphite – LIPON – LCO modeled system with a 1C current. (a)** Potential vs time. **(b)** State of charge (soc) of the electrodes. **0** at the initial stage. **i** At the beginning of the charge**. ii** During charge. **iii** At the end of the charge and the beginning of the discharge. **iv** During discharge **v** At the end of discharge.

Accepted Manuscript
For Review Only

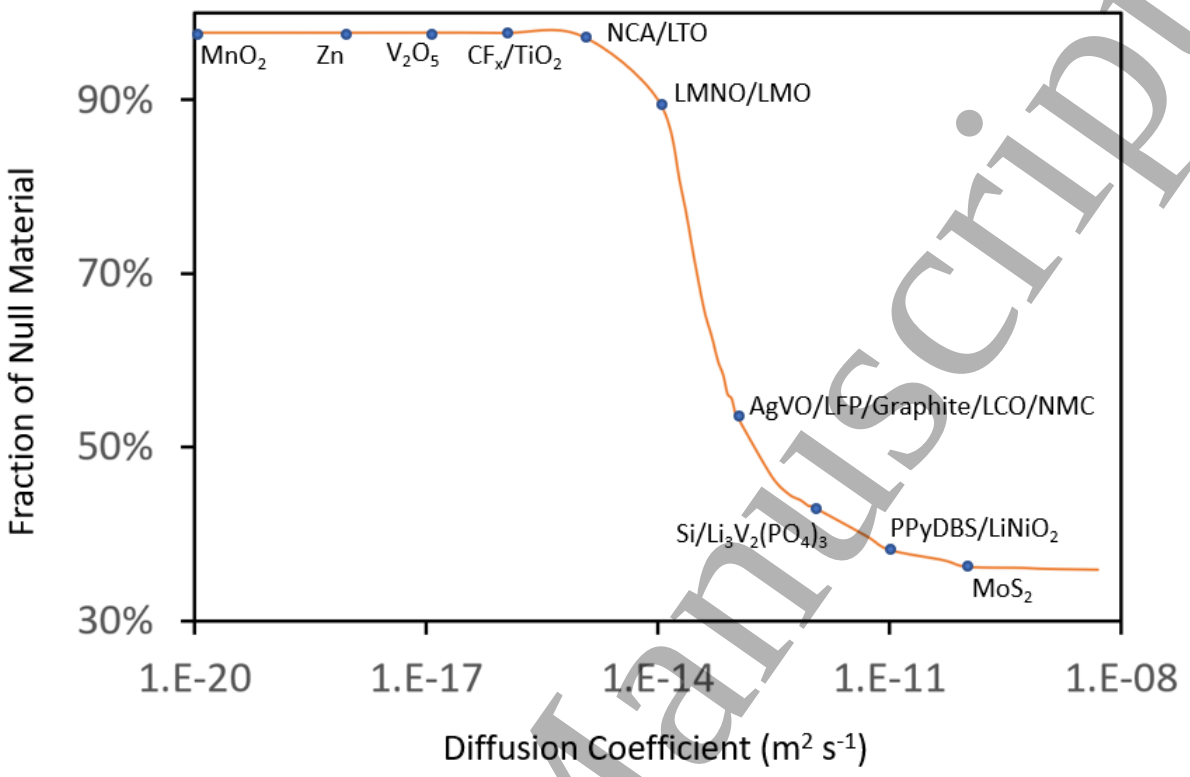


**Figure 4: Presentation of the percentage of Null material as a function of $Li^+$ diffusion coefficient in electrodes at a 1C kinetic. (a)** for diffusion coefficients from $10^{-20}$ to $10^{-12}$ $m^2$ $s^{-1}$ **(b)** for a diffusion coefficient from $10^{-12}$ to $10^{-10}$ $m^2$ $s^{-1}$. **(c)** for diffusion coefficient from $10^{-20}$ to $10^{-15}$ $m^2$ $s^{-1}$. A list of state-of-the-art electrode material are presented on the curve.

Accepted Manuscript
View Only

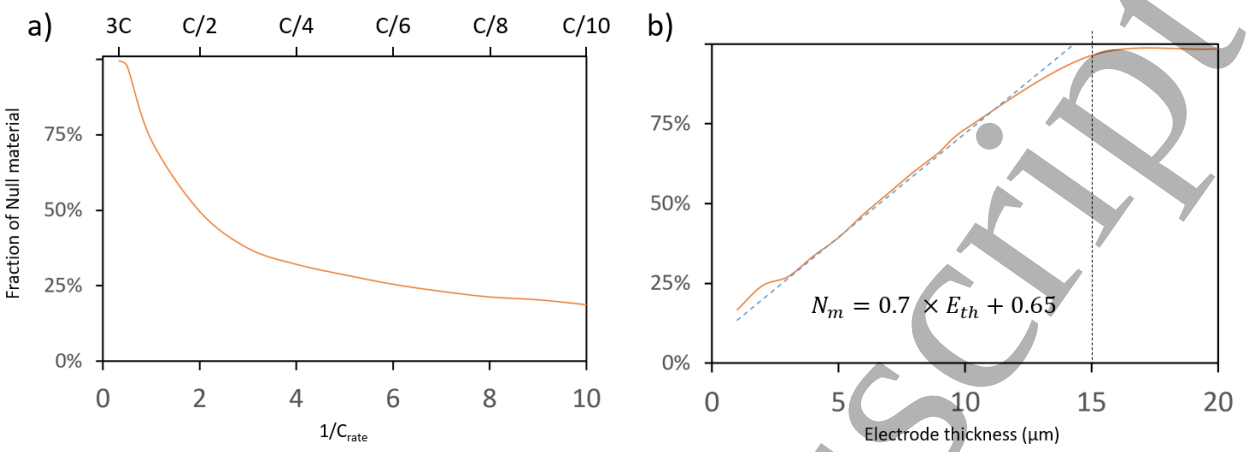


**Figure 5: Impact of Crate and electrode thickness on charge heterogeneity in the cell. a)** Fraction of null material vs charge factor extracted from modelisation data. **b)** fraction of null material vs electrode thickness extracted from model data (plein orange) and fitting curve (blue dashes) with associated equation.

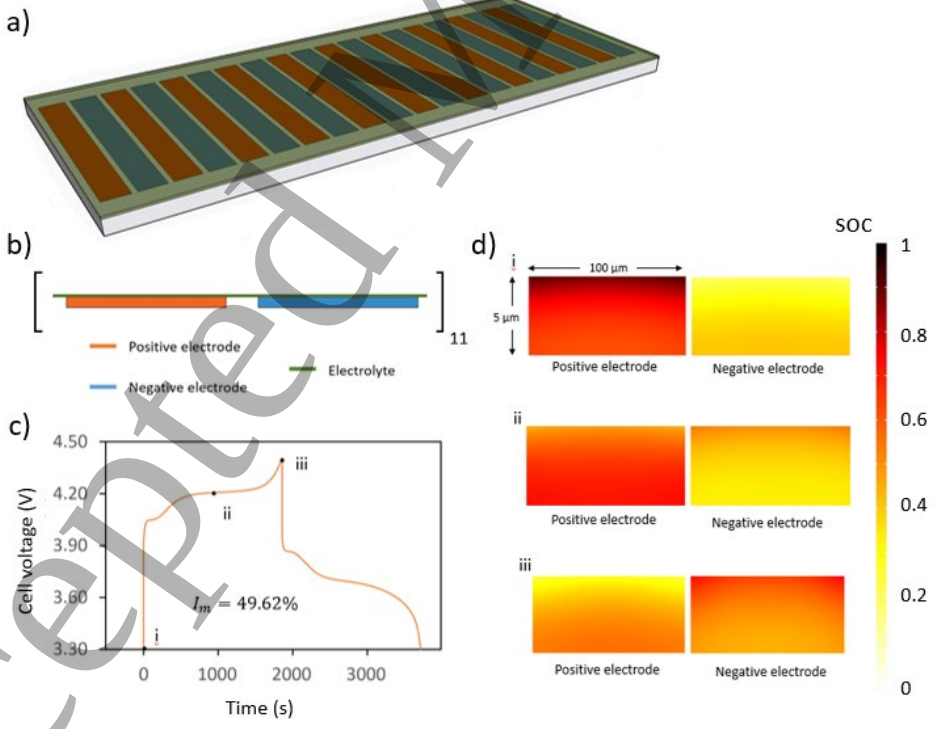


**Figure 6: Charge heterogeneity in a MEES with planar geometry. (a)** 3D model of the planar structure. **(b)** 2D model of the planar structure at a 1:20 aspect ratio. **(c)** Potential curve versus time





Accepted Manuscript For Review

over a complete charge-discharge cycle and percentage of Null material associated with the system **(d)** State of charge of the positive (left) and negative (right) electrodes **i.** at the beginning of the charge cycle **ii.** in the middle of the charge cycle **iii.** at the end of the charge cycle with a 1:20 aspect ratio.

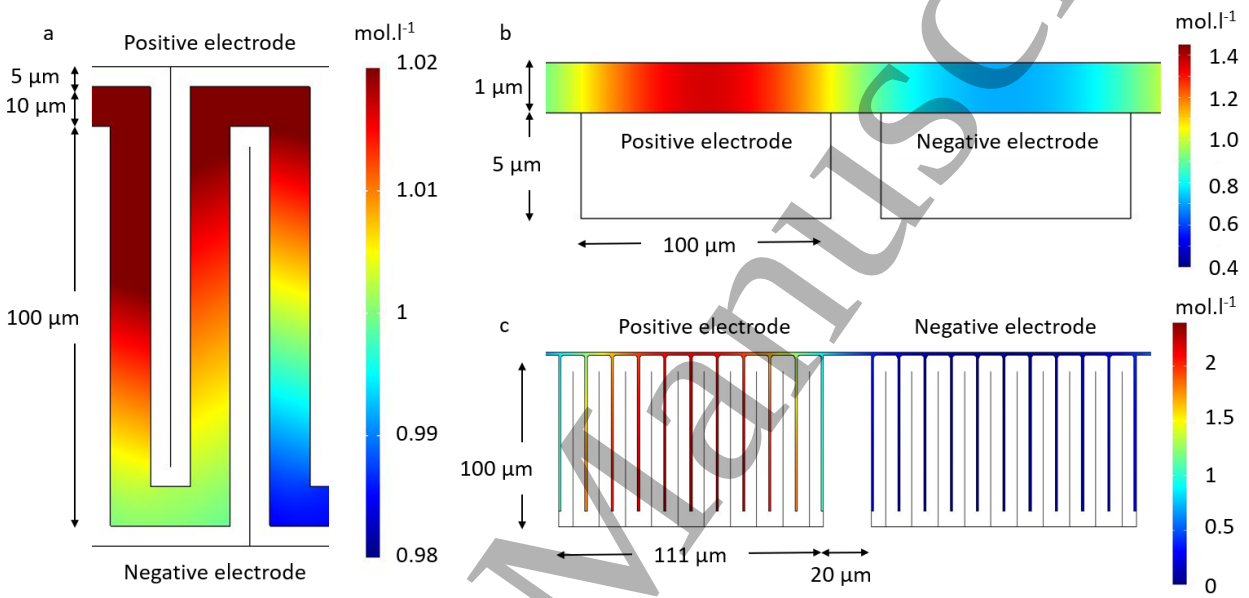


**Figure 7: disparity of ionic concentration in the different configuration with a LCO-$LiPF_6$ gel-Graphite cell. (a)** Lithium-ion concentration in the electrolyte for the trench model. **(b)** lithium-ion concentration in the electrolyte in the interdigit 2D model. **(c)** lithium-ion concentration of the electrolyte in the 3D interdigitated model with micropillar as a 3D efficient scaffold.

Accepted Manuscript
For Review Only